Journal of Solid State Chemistry 182 (2009) 3188–3194

Contents lists available at ScienceDirect

Journal of Solid State Chemistry

journal homepage: www.elsevier.com/locate/jssc

Carbon-assisted morphological manipulation of CdS nanostructures and their cathodoluminescence properties

Meng Zhang [a,b], Tianyou Zhai [a], Xi Wang [a,b], Qing Liao [a], Ying Ma [a,*], Jiannian Yao [a,*]

[a] Beijing National Laboratory for Molecular Science (BNLMS), Key Laboratory of Photochemistry, Institute of Chemistry, Chinese Academy of Sciences, Beijing 100190, PR China
[b] Graduate School of the Chinese Academy of Sciences, Beijing 100049, PR China

ARTICLE INFO

Article history:
Received 16 July 2009
Received in revised form
22 August 2009
Accepted 29 August 2009
Available online 6 September 2009

Keywords:
Cadmium sulfide
Cathodoluminescence
Carbon
Semiconductors
Thermal evaporation

ABSTRACT

CdS nanostructures with different morphologies and sizes were successfully fabricated through a facile and effective carbon-assisted thermal evaporation method. Through simply changing the positions of silicon substrates, the temperatures and the effects of carbon in different zones were modified, and thus the morphologies of CdS nanostructures were varied from multipods to nanobrushes to nanocups. These nanostructures were characterized by scanning electron microscopy (SEM), transmission electron microscopy (TEM), energy-dispersive X-ray spectrometry (EDS), X-ray powder diffraction (XRD) and Raman spectroscopy. Cathodoluminescence (CL) measurement shows that the as-grown CdS nanostructures display different luminescent properties. CdS multipods and nanocups show mainly green emission centered at ~496 nm. However, nanobrushes exhibit predominant red emission band peaking at ~711 nm. These interesting results show that carbon not only affected the growth process but also influenced the properties of CdS nanostructures.

1. Introduction

It is well known that the utilization of nanostructure-based materials greatly depends on the morphology of the nanostructures (e.g. size and shape) [1–3], and much effort has been made in the synthesis of a wide range of complex nanomaterials for their potential novel optical and electronic properties [4–15]. As an important II–VI semiconductor with a band gap of 2.52 eV at room temperature, CdS is one of the most important electronic and optoelectronic materials with prominent applications in nonlinear optical devices, flat panel displays, light emitting diodes, laser, logic gates, transistors, etc [16,17]. It is also an active optical waveguide material and electrically driven lasing material, which may find wide applications in telecommunications, data storage and near-field optical lithography [18,19]. Several complex CdS micro/nanostructures have been fabricated by chemists for their potential applications as interconnections in the "bottom-up" self-assembly approach toward future nanocircuits and nanodevices. For example, we have recently fabricated the rocket-like tetrapodal CdS nanorods via a one-step seed-epitaxial metal-organic chemical vapor deposition approach by thermal decomposition of $Cd(S_2CNEt_2)_2$ powders [20]. Multi-armed CdS nanorods were synthesized by Jun et al. using thermal decomposition of $Cd(S_2CNEt_2)_2$ in hexadecylamine [21]. Liu reported the synthesis of a sea-urchinlike CdS nanorod-based material in ethylenediamine solution [22]. In addition, other CdS nanostructures, such as netted sphere-like CdS structures [23], tetrapods and hexagonal nanoprisms [24], branched nanowires, and fractal nanotrees [25] have also been prepared. In all above cases, however, harsh conditions such as reactions in organic solvents which are environmentally unfriendly or metal-organic precursors that are difficult to access are normally required. Therefore, seeking new and versatile synthetic routes to synthesize complex CdS nanostructures especially with manipulable morphology and property is still important.

In this contribution, we report a facile and effective carbon-assisted thermal evaporation method to synthesize CdS nanostructures. Through simply changing the positions of silicon substrates, the temperatures and the effects of carbon in different zones can be modified, and the morphologies of CdS nanostructures consequently varied from multipods to nanobrushes to nanocups. To the best of our knowledge, the as-grown CdS nanocups and nanobrushes have not been reported. As for CdS multipods, however, most of reported ones have been prepared by solution chemistry methods [26,27]. Furthermore, room-temperature cathodoluminescence (CL) studies show that the as-grown CdS nanostructures display very different optical properties. CdS multipods and nanocups show mainly green emission centered at ~496 nm; nevertheless, nanobrushes chiefly exhibit red emission band peaking at ~711 nm. This method may also offer an easy way to prepare C doped CdS nanostructures.

* Corresponding authors. Fax: +86 10 82616517.
E-mail addresses: yingma@iccas.ac.cn (Y. Ma), jnyao@iccas.ac.cn (J. Yao).

0022-4596/$ - see front matter © 2009 Elsevier Inc. All rights reserved.
doi:10.1016/j.jssc.2009.08.028

2. Experimental section

2.1. Preparation

The CdS nanostructures were synthesized in a horizontal tube furnace. In short, 0.2 g perylene (Alfa Aesar, 98%) and 0.6 g commercial-grade CdS powder were placed in the upstream and center region of quartz tube, respectively. Silicon wafers cleaned by standard procedure were fixed on the top of the downstream quartz tube using a high temperature sealant (Fig. 1). Cooling water flows inside cover caps to achieve a reasonable temperature gradient in this tube. After high purity N_2 gas (99.99%) at a flow rate of 120 sccm (standard cubic centimeter per minute) was introduced into the system for 30 min to purge oxygen, the furnace was raised to 850 °C in 40 min and held at this temperature for 15 min before cooled to room temperature. Finally the products (CdS multipods, nanobrushes and nanocups) were collected in zone I, II and III of the quartz tube, respectively.

2.2. Characterizations

The as-synthesized products were characterized by scanning electron microscopy (SEM, Hitachi F-4800) equipped with energy-dispersive X-ray spectrometry (EDS), transmission electron microscope (TEM, JEOL JEM-2010), high resolution TEM (HRTEM, Philips Tecnai F-30), and X-ray diffraction (XRD, Philips X′Pert PRO MPD) with Cu$K\alpha$ as the radiation source. The Raman spectra were recorded in the backscattering geometry by using a Renishaw-2000 Raman spectrometer with the 514.5 nm line of an Ar ion laser as the excitation source. Luminescent spectra of these nanostructures were measured at room temperature by a cathodoluminescence (CL) system installed on the SEM (SEM, Quanta 200F).

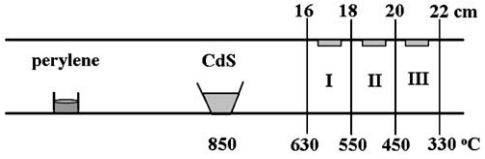

Fig. 1. Schematic diagram of the three distinctive growth zones inside of the quartz tube. The deposition widths and temperature ranges of these zones are also shown.

3. Results and discussion

3.1. Morphologies and structures of CdS products

On the basis of SEM images, three distinctive zones were identified (Fig. 1). The morphologies of CdS structures changed from multipods in zone I (630–550 °C, 16–18 cm from the center) to nanobrushes in zone II (550–450 °C, 18–20 cm), and finally nanocups in zone III (450–330 °C, 20–22 cm).

Fig. 2a shows a typical SEM image of the as-synthesized multipods, which consist of monopods, bipods, tripods and tetrapods. Fig. 2b, c display high-magnification SEM images of some tripods. The diameter and length of each pod are about 600 nm and 2.5 μm, respectively. These multipods have rough surfaces, and change little in morphology when deposition temperature ranges from 630 to 550 °C. The energy dispersive X-ray spectrum (EDS) in Fig. 2c shows that Cd and S elements are in an atomic ratio close to 1:1 (1.01:1.00), nevertheless C element is not detected possibly due to the very low content of carbon in this product. The detailed microstructures of the CdS multipods were further characterized by transmission electron microscopy (TEM). For clarity, Fig. 2d gives a TEM image of one pod in the tripod, obviously the tip end of the pod is irregular and the diameter

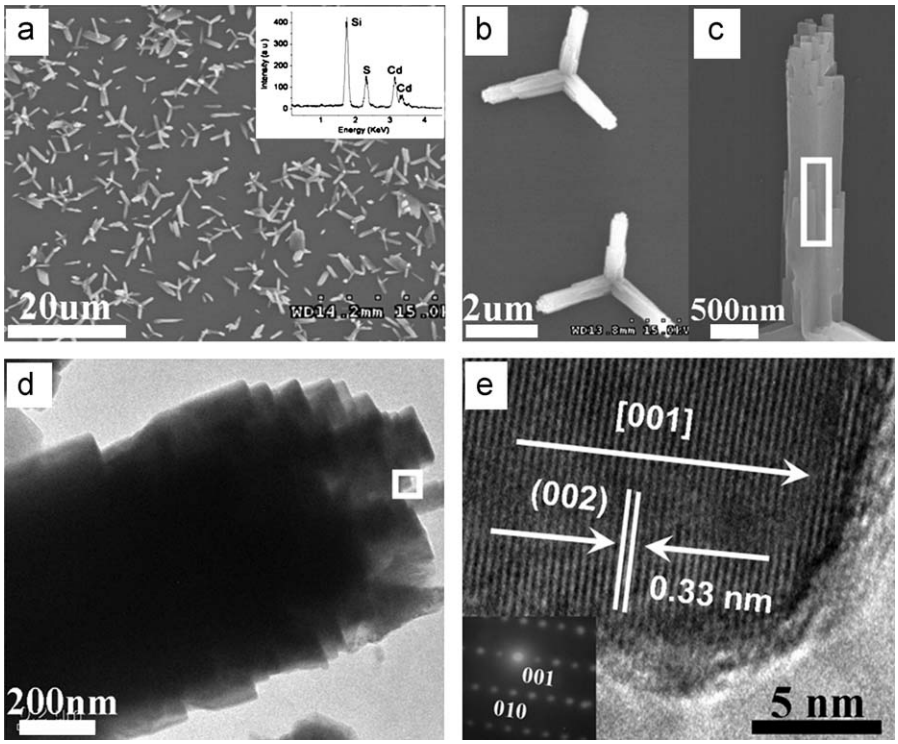

Fig. 2. CdS multipods formed in zone I. (a) SEM image of multipods and EDS spectrum of tripods (inset) corresponding to rectangular area in Fig. 2c; (b, c) high-magnification SEM images of the tripods; (d) TEM image of one pod in the CdS tripod; (e) HRTEM image and the corresponding SAED pattern (inset) of the pod showing the pod grows along [001].

of the pod is about 600 nm, in accordance with the SEM results. Fig. 2e is a HRTEM image of the CdS multipod, indicating a perfect wurtzite structure with the corresponding selected area electron diffraction (SAED) displayed in the inset. The fringe spacing shown in the image is about 0.33 nm, corresponding to the (002) plane of wurtzite CdS, which is consistent with those reported in the literatures [20,28,29]. As can be derived from the SAED pattern and HRTEM image, the pod has a single-crystalline structure and grows along the [001] direction.

With the decrease of substrate temperature, the morphology of CdS structures changed significantly. SEM images show that nanobrushes were formed in zone II, in contrast to the multipods formed in zone I. The low-magnification SEM image as shown in Fig. 3a demonstrates that the nanobrushes with relatively high yield distribute uniformly. High-magnification SEM images (Fig. 3b, c) show that the upper section of nanostructures consists of numerous arrayed nanowires with various lengths and diameters ranging from 50 to 80 nm. Fig. 3d gives the EDS result of the nanobrushes. Compared with that of the multipods, a mass of carbon was detected, and the content of carbon is about 34.09%. Fig. 3e displays a TEM image of a single nanobrush with the diameter of about 500 nm and length of about 1.5 μm. The corresponding SAED pattern (inset of Fig. 3e) reveals that the nanobrush is polycrystalline in nature. Fig. 3f is a HRTEM image of a single nanowire grown on the nanobrush, and the fringe spacing shown in the image is about 0.21 nm, which agrees well with the (110) lattice plane of the hexagonal CdS.

With further decrease of the substrate temperature (zone III of the quartz tube), the shape of products changed from nanobrushes to nanocups. Fig. 4a depicts a low-magnification image of cup-like CdS nanostructures, which demonstrates that the products cover nearly the whole Si substrate. From the high-magnification images (Fig. 4b, c), we can find that the nanocups are of hexagonal shape with very smooth surface. The average diameter, height and wall thickness of the cup-like structures are respectively ~350, ~500 and ~80 nm, and the hexagonal bottom surface of a nanocup is exhibited in the upper right inset in Fig. 4b. EDS analysis (Fig. 4d) proves the existence of C element in this product. The percentage of C element (45.09%) in nanocups is much higher than that in multipods (not detected) and nanobrushes (34.09%), suggesting more carbon involved in nanocup structures. Fig. 4e shows a typical low-magnification TEM image of the nanocups, and the diameter and height of the nanocups are about ~180 and ~220 nm, respectively. Fig. 4f is a

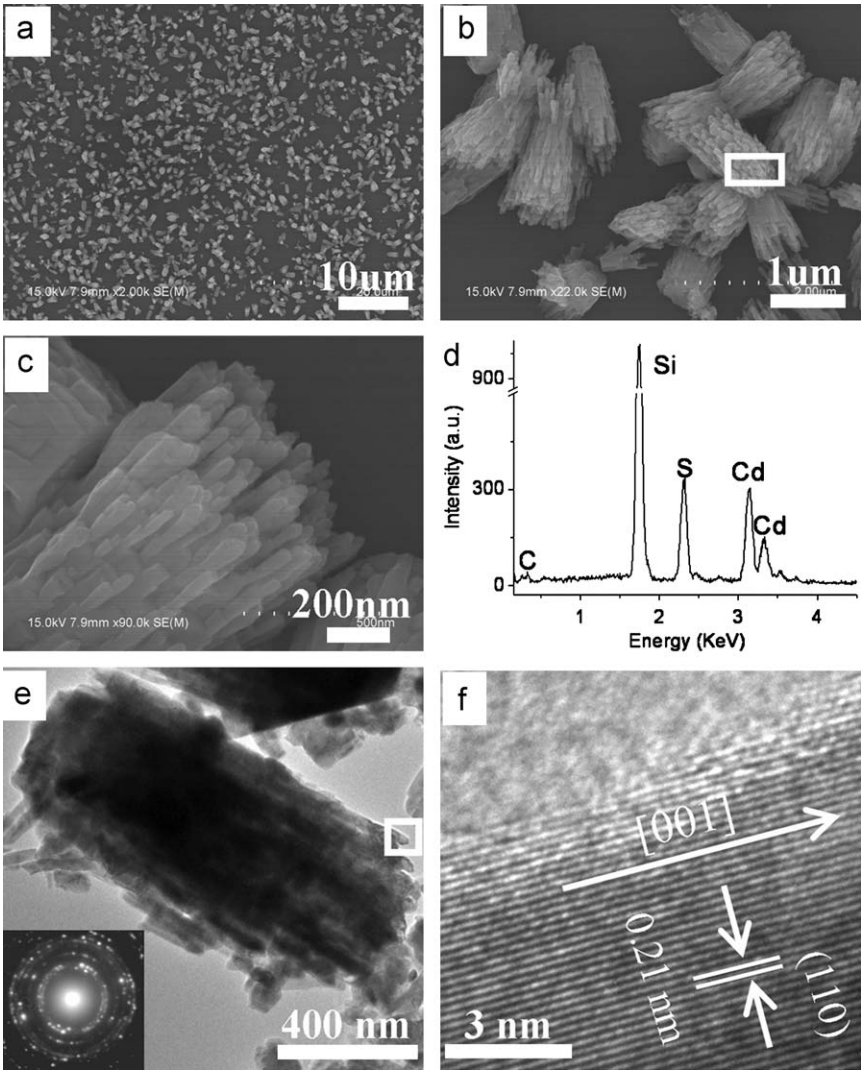

Fig. 3. CdS nanobrushes formed in zone II. (a, b, c) SEM images of the CdS nanobrushes; (d) EDS spectrum of the CdS nanobrushes; (e) TEM image and SAED pattern (inset) of an individual CdS nanobrush; (f) HRTEM image of the CdS nanobrush corresponding to white square region marked in Fig. 3e.

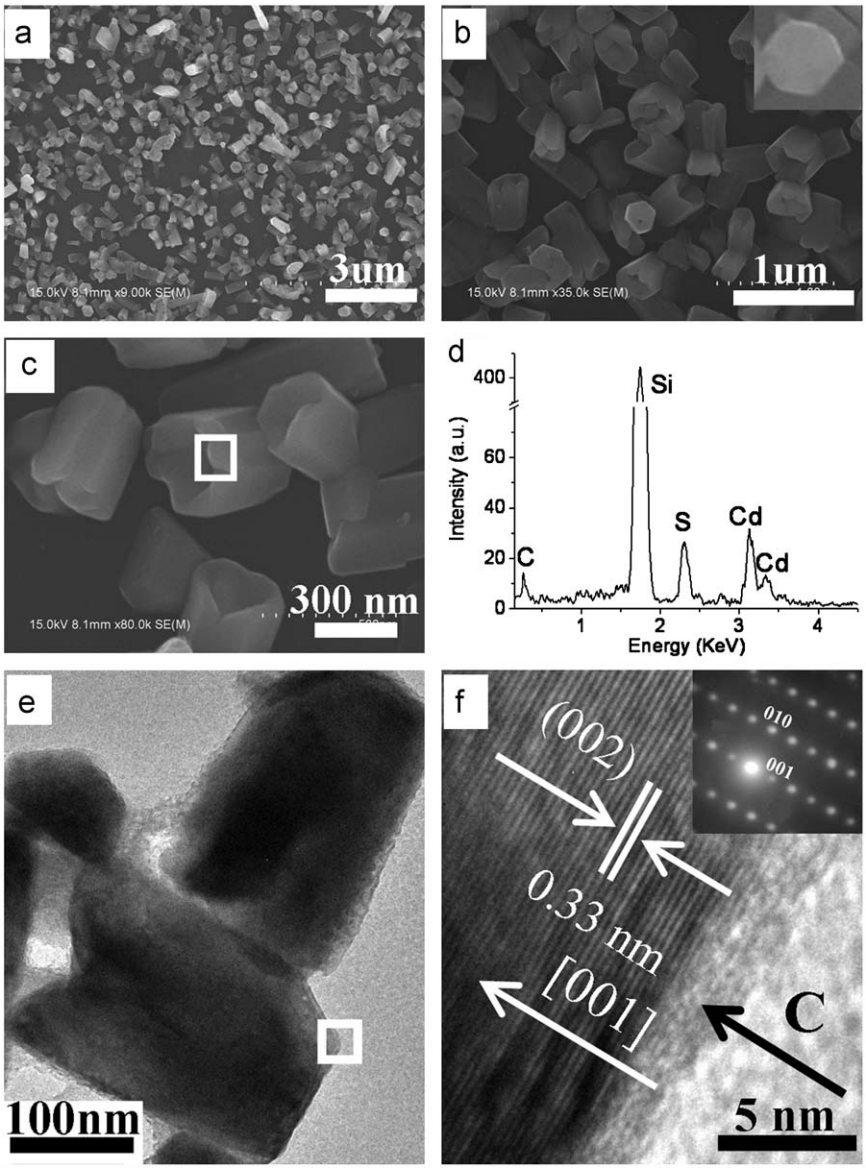

Fig. 4. CdS nanocups formed in zone III. (a, b, c) SEM images of the CdS nanocups; (d) EDS spectrum of the CdS nanocups; (e) TEM image of nanocups; (f) HRTEM image and corresponding SAED pattern (inset) of a nanocup. A layer of carbon is observed clearly.

HRTEM image of a nanocup, which shows that the nanocup has an interplanar spacing of ca. 0.33 nm, corresponding to the (002) plane of hexagonal CdS. In addition, the corresponding ED pattern (inset) displays that the nanocup has a single-crystalline structure and a carbon layer is clearly observed in this HRTEM image.

The X-ray diffraction (XRD) patterns of these structures and the standard XRD pattern for CdS (Joint Committee for Power Diffraction Standards, JCPDS Card, No. 80–0006) are presented in Fig. 5. All the diffraction peaks of the three nanostructures can be indexed as a hexagonal wurtzite CdS with the lattice constants of a=4.121 Å, and c=6.682 Å. Curve a shows the XRD pattern of the multipods. Except characteristic peaks of wurtzite CdS, No other peaks from impurities were detected. The sharp diffraction peaks indicate the good crystallinity of the prepared crystals. Compared with those of multipods, less and weaker diffraction peaks are observed in the nanobrush (curve b) indicating the relatively poor crystallinity of this product. In addition, a broad peak at 2θ=17–31° confirms that amorphous carbon exists in the

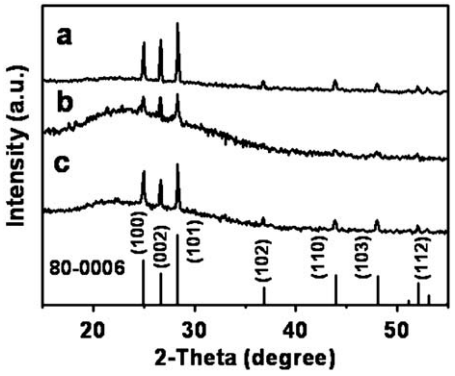

Fig. 5. XRD patterns of CdS multipods (a), nanobrushes (b) and nanocups (c), which were obtained at different zones in the quartz tube, respectively. The vertical lines at the bottom in the figure correspond to the standard XRD pattern of wurtzite CdS (JCPDS No. 80–0006).

nanobrush [30]. Similar to nanobrushes, a broad peak with weaker intensity at 2θ=17–31° is also observed in the nanocups (curve c) demonstrating the existence of amorphous carbon. Nevertheless diffraction peaks attributed to CdS are very sharp, suggesting the good crystallinity of nanocups.

Fig. 6 shows the Raman spectra of these CdS nanostructures measured at room temperature. Three sharp peaks and two weak broad bands can be observed in all of the spectra. The two peaks located at 301 and 603 cm^{-1} can be assigned to the first-order and second-order longitudinal optical phonon bands of CdS, respectively [31–33]. The Raman band at 1349 cm^{-1} (D-band) associates with the vibration of carbon atoms with dangling bonds at the plane termination of disordered graphite or glass carbon, and the one at 1586 cm^{-1} (G band) corresponds to an E_{2g} mode of graphite and relates to the vibration of sp^2-bonded carbon atoms in a two-dimensional graphite layer [34]. The peak at 519 cm^{-1} arises from the Si substrate [32] and the carbon signals of multipods in Raman spectrum may be attributed to trace carbon on the Si substrate and multipods.

3.2. Growth mechanism

We believe carbon produced by pyrolysis of perylene plays a crucial role in the growth progress of nanobrushes and nanocups because similar results could also be acquired by using polymethyl methacrylate as the carbon precursor. However, without carbon precursor, only CdS multipods could be obtained as shown in Fig. 7, in which the size varies with different multipods. Even if carbon powder was used as the precursor or carbon particles covered single-crystal silicon wafers were used as the substrates, CdS multipods were the only product. Due to the relatively higher temperature in the zone I of quartz tube, trace amount of carbon was deposited and involved in the growth process of CdS nanostructures, which was verified by the EDS measurement. Multipods including mono-, bi-, tri- and tetrapods were obtained in this zone. Similar to the solution grown nanocrystals, CdS multipods may be formed by continuous growth of wurtzite arms from four equivalent (111) facets of a sphalerite nucleus or further growth of the initial nucleus generated by eight wurtzite domains connected to each other through twin boundaries [35]. We are not sure which model is dominant in this process since we could not get detailed TEM investigations due to the large size of the multipods. For wurtzite CdS, it favors the growth along the [001] axis [20,27] as confirmed by the HRTEM image of Fig. 2e. With the temperature decreasing (zone II), more carbon was deposited and involved in the growth process of CdS nanostructures, as confirmed by EDS measurement with the content of C element being 34.09%. These carbon particles scattered on partial surface of the pre-grown CdS structures and hindered new arriving CdS(g) from adsorbing on these sites [36,37], which may result in considerable defects and poor crystallinity in the structures. Moreover, selective continuous growth of CdS on some sites of the pre-grown structures led to the formation of numerous nanowires arrays. These are consistent with the SEM images and XRD pattern. CdS nanocups were deposited in zone III of the quartz tube. With the further decrease of temperature, more carbon (45.09%) was deposited and formed carbon sheaths on the surface of pre-grown CdS structures as indicated in Fig. 4f. Carbon sheaths blocked further crystal development in these locations, therefore new arriving CdS species preferred to adsorb onto the edges of the pre-grown structures, which inclined to form cup-like structures [38]. The possible growth mechanism of CdS multipods, nanobrushes and nanocups is illustrated in Fig. 8.

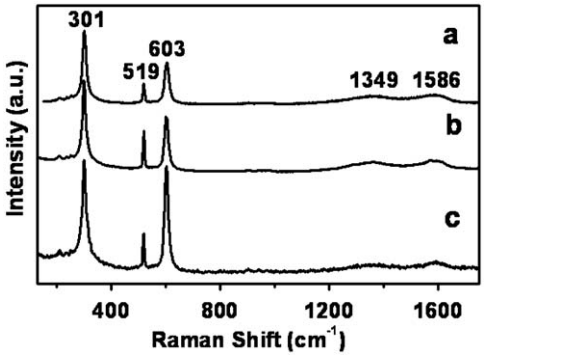

Fig. 6. Raman spectra of multipods (curve a), nanobrushes (curve b) and nanocups (curve c).

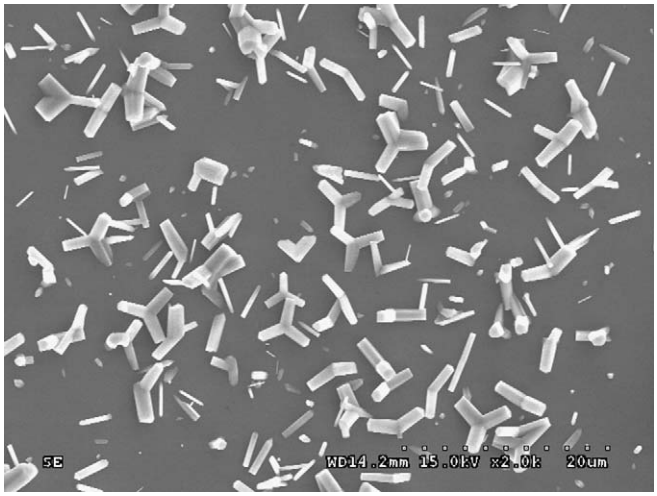

Fig. 7. SEM image of CdS multipods acquired in the absence of perylene.

3.3. Optical properties

Cathodoluminescence (CL) is one of the most widely used techniques to investigate optical properties of nanostructures because of its high spatial resolution and surface sensitivity [39]. In this work, the nanoscale CL spectroscopy and CL imaging were conducted at an acceleration voltage of 15 KV. SEM and CL images were recorded at room temperature and shown in Fig. S1 in

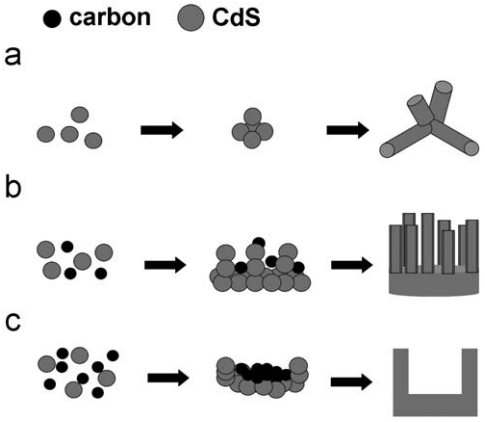

Fig. 8. Schematic illustration of the growth mechanisms for CdS multipods (a), nanobrushes (b) and nanocups (c).

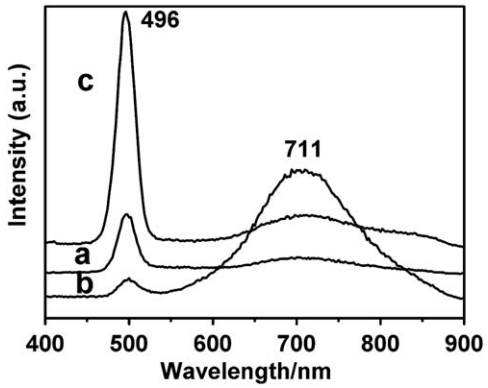

Fig. 9. Room-temperature cathodoluminescence spectra of CdS multipods (curve a), nanobrushes (curve b) and nanocups (curve c) obtained with a focused electron beam at an accelerating voltage of 15 kV.

supporting information. The CL spectra of CdS multipods, nanobrushes and nanocups were respectively, recorded as curves a, b and c in Fig. 9. All of the CdS nanostructures exhibit green emission centered at ~496 nm and broad red emission centered at ~711 nm.

Generally, two emission bands can be observed for CdS nanostructures: excitonic and trapped state luminescence, respectively [40]. The excitonic emission is located near the absorption edge of the particles and may arise from the free electron-hole recombination or/and shallowly trapped electron-hole pairs [40,41]. The trapped state emission can be ascribed to the deep level emission (DL) that is related to impurities, structure defects, nonstoichiometric sites or the excess of sulfur or cadmium vacancies at the interface [42–44]. Zou et al. [42] reported a broad band at ~502.5 nm attributed to the spontaneous exciton transition at the bandedge for CdS nanowires. A band gap emission at 504.5 nm and a broad emission from defects at 600–800 nm were observed in CdS nanoribbons [45]. CdS nanowires prepared by Cao et al. [46] showed a predominant band-edge emission at ~426 nm and a weaker trap-state green-light emission at ~530 nm in wavelength. Fan and Yang [47] found that CdS hierarchical nanotube arrays also exhibited two emission peaks. The sharp and narrow green emission peak near 480 nm was attributed to the band-gap emission, whereas the broad red emission peak between 600 and 720 nm was trapped emission due to the excess of sulfur at the surface defects.

As shown in Fig. 9a, multipods show an intensive emission peak centered at ~496 nm with the full width at half-maximum (FWHM) of 23 nm, as well as a broad and weak band ranging from 600 to 850 nm and centered at 711 nm. The peak at ~496 nm may be assigned to band edge (BE) emission of CdS, whereas the broad red band at ~711 nm can be ascribed to the deep level (DL) emission, according to above discussions. The intensity ratio of deep level to band edge emission (I_{DL}/I_{BE}) is ~0.5. For nanobrushes (curve b), the relatively intensity of two emission bands varied greatly, the red emission band becomes predominant emission in nanobrushes with the ratio of I_{DL}/I_{BE} being ~5.8. Fig. 9c shows that the intensity ratio of I_{DL}/I_{BE} is ~0.3 for nanocups. The different luminescent properties of the three nanostructures are reasonable. The nanobrushes composed of numerous nanowires have larger surface-aspect ratios and more defects, as shown in XRD and HRTEM results, or/and deep levels introduced by C substitution of S [48], which will greatly enhance the DL emission. Whereas, the formation of separate carbon sheaths and high-quality single-crystal structure can lead to stronger BE emission and weaker DL emission of the nanocups.

4. Conclusions

In summary, by employing a simple carbon-assisted thermal evaporation method, various CdS nanostructures (multipods, nanobrushes and nanocups) have been successfully synthesized in different zones of the quartz tube. Carbon produced by pyrolysis of perylene plays a critical role in the formation of different nanostructures. Multipods and nanocups display single-crystalline structure; nevertheless the nanobrush shows a poly-crystalline structure. Cathodoluminescence technique is used to characterize the luminescence properties of CdS nanostructures. All nanostructures show two distinct emission peaks. One centers at ~496 nm and the other centers at ~711 nm. Multipods and nanocups show mainly green emission. In contrast, nanobrushes exhibit predominant red emission, which may be due to the increased defects of polycrystalline structure or/and deep levels introduced by C doping. These interesting results show that carbon not only affected the growth process but also influenced the properties of CdS nanostructures. The as-prepared nanostructures may have potential applications in future optoelectronic nanodevices due to their interesting optical properties. This method may also offer an easy way to prepare C doped semiconductor nanostructures.

Acknowledgments

This work was supported by the National Natural Science Foundation of China (Grant nos. 20733006, 20871117), the CAS/SAFEA International Partnership Program for Creative Research Teams, and the National Basic Research Program of China (2006CB806200, 2007CB936402).

Appendix A. Supplementary Materials

The online version of this article contains additional supplementary data. Please visit doi:10.1016/j.jssc.2009.08.028.

References

[1] P.C. Ohara, J.R. Heath, W.M. Gelbart, Angew. Chem. Int. Ed 36 (1997) 1078.
[2] T. Vossmeyer, E. Delonno, J.R. Heath, Angew. Chem. Int. Ed. 36 (1997) 1080.
[3] H.Q. Yan, R.R. He, J. Pham, P.D. Yang, Adv. Mater. 15 (2003) 402.
[4] X. Fan, X.M. Meng, X.H. Zhang, W.S. Shi, W.J. Zhang, J.A. Zapien, C.S. Lee, S.T. Lee, Angew. Chem. Int. Ed. 45 (2006) 2568.
[5] G.Z. Shen, Y. Bando, D. Golberg, Appl. Phys. Lett. 88 (2006) 123107.
[6] P.X. Gao, Z.L. Wang, J. Am. Chem. Soc. 125 (2003) 11299.
[7] B. Liu, H.C. Zeng, J. Am. Chem. Soc. 126 (2004) 16744.
[8] T.R. Zhang, W.J. Dong, M. Keeter-Brewer, S. Konar, R.N. Njabon, Z.R. Tian, J. Am. Chem. Soc. 128 (2006) 10960.
[9] M. Shim, P. Guyot-Sionnest, J. Am. Chem. Soc. 123 (2001) 11651.
[10] H.D. Yu, Z.P. Zhang, M.Y. Han, X.T. Hao, F.R. Zhu, J. Am. Chem. Soc. 127 (2005) 2378.
[11] J. Joo, S.G. Kwon, J.H. Yu, T. Hyeon, Adv. Mater. 17 (2005) 1873.
[12] M. Umetsu, M. Mizuta, K. Tsumoto, S. Ohara, S. Takami, H. Watanabe, I. Kumagai, T. Adschiri, Adv. Mater. 17 (2005) 2571.
[13] J.H. Choy, E.S. Jang, J.H. Won, J.H. Chung, D.J. Jang, Y.W. Kim, Appl. Phys. Lett. 84 (2004) 287.
[14] Y. Lv, C.P. Li, L. Guo, Q.X. Wang, R.M. Wang, H.B. Xu, S.H. Yang, X.C. Al, J.P. Zhang, Appl. Phys. Lett. 87 (2005) 163103.
[15] L. Manna, D.J. Milliron, A. Meisel, E.C. Scher, A.P. Alivisatos, Nat. Mater. 2 (2003) 382.
[16] H. Pan, C.K. Poh, Y. Zhu, G. Xing, K.C. Chin, Y.P. Feng, J. Lin, C.H. Sow, W. Ji, A.T.S. Wee, J. Phys. Chem. C 112 (2008) 11227.
[17] T.Y. Zhai, X.S. Fang, Y. Bando, Q. Liao, X.J. Xu, H.B. Zeng, Y. Ma, J.N. Yao, ACS Nano 3 (2009) 949.
[18] X.F. Duan, Y. Huang, R. Agarwal, C.M. Lieber, Nature 421 (2003) 241.
[19] A.L. Pan, D. Liu, R.B. Liu, F.F. Wang, X. Zhu, B.S. Zou, Small 1 (2005) 980.
[20] T.Y. Zhai, Z.J. Gu, H.Z. Zhong, Y. Dong, Y. Ma, H.B. Fu, Y.F. Li, J.N. Yao, Cryst. Growth Des. 7 (2007) 488.
[21] Y.W. Jun, S.M. Lee, N.J. Kang, J. Cheon, J. Am. Chem. Soc. 123 (2001) 5150.

[22] X.H. Liu, Mater. Chem. Phys. 91 (2005) 212.
[23] P.T. Zhao, K.X. Huang, Cryst. Growth Des. 8 (2008) 717.
[24] H.B. Chu, X.M. Li, G.D. Chen, W.W. Zhou, Y. Zhang, Z. Jin, J.J. Xu, Y. Li, Cryst. Growth Des. 5 (2005) 1801.
[25] W.T. Yao, S.H. Yu, S.J. Liu, J.P. Chen, X.M. Liu, F.Q. Li, J. Phys. Chem. B 110 (2006) 11704.
[26] F. Gao, Q.Y. Lu, S.H. Xie, D.Y. Zhao, Adv. Mater. 14 (2002) 1537.
[27] J. Joo, H.B. Na, T. Yu, J.H. Yu, Y.W. Kim, F.X. Wu, J.Z. Zhang, T. Hyeon, J. Am. Chem. Soc. 125 (2003) 11100.
[28] J. Zheng, X.B. Song, N. Chen, X.G. Li, Cryst. Growth Des. 8 (2008) 1760.
[29] G.Z. Shen, C.J. Lee, Cryst. Growth Des. 5 (2005) 1085.
[30] M. Noh, Y. Kwon, H. Lee, J. Cho, Y. Kim, M.G. Kim, Chem. Mater. 17 (2005) 1926.
[31] H. Pan, G.C. Xing, Z.H. Ni, W. Ji, Y.P. Feng, Z. Tang, D.H.C. Chua, J. Lin, Z.X. Shen, Appl. Phys. Lett. 91 (2007) 193105.
[32] H.M. Fan, X.F. Fan, Z.H. Ni, Z.X. Shen, Y.P. Feng, B.S. Zou, J. Phys. Chem. C 112 (2008) 1865.
[33] L. Zeiri, I. Patla, S. Acharya, Y. Golan, S. Efrima, J. Phys. Chem. C 111 (2007) 11843.
[34] X.P. Shen, Z.Y. Jiang, C.L. Gao, Z. Xu, Z.X. Xie, L.S. Zheng, J. Mater. Chem. 17 (2007) 1326.
[35] L. Carbone, S. Kudera, E. Carlino, W.J. Parak, C. Giannini, R. Cingolani, L. Manna, J. Am. Chem. Soc. 128 (2006) 748.
[36] Y.C. Zhu, Y. Bando, D.F. Xue, D. Golberg, J. Am. Chem. Soc. 125 (2003) 16196.
[37] X.S. Fang, Y. Bando, G.Z. Shen, C.H. Ye, U.K. Gautam, P. Costa, C.Y. Zhi, C.C. Tang, D. Golberg, Adv. Mater. 19 (2007) 2593.
[38] Y.S. Fu, X.W. Du, J. Sun, Y.F. Song, J. Liu, J. Phys. Chem. C 111 (2007) 3863.
[39] D.D.D. Ma, S.T. Lee, P. Mueller, S.F. Alvarado, Nano Lett. 6 (2006) 926.
[40] Y.W. Wang, G.W. Meng, L.D. Zhang, C.H. Liang, J. Zhang, Chem. Mater. 14 (2002) 1773.
[41] J.H. Zhan, X.G. Yang, D.W. Wang, S.D. Li, Y. Xie, Y. Xia, Y.T. Qian, Adv. Mater. 12 (2000) 1348.
[42] W.C. Zhou, A.L. Pan, Y. Li, G.Z. Dai, Q. Wan, Q.L. Zhang, B.S. Zou, J. Phys. Chem. C 112 (2008) 9253.
[43] C.R. Wang, K.M. Ip, S.K. Hark, Q. Li, J. Appl. Phys. 97 (2005) 054303.
[44] T. Gao, T.H. Wang, J. Phys. Chem. B 108 (2004) 20045.
[45] X. Fan, M.L. Zhang, I. Shafiq, W.J. Zhang, C.S. Lee, S.T. Lee, Cryst. Growth Des. 9 (2009) 1375.
[46] H.Q. Cao, G.Z. Wang, S.C. Zhang, X.R. Zhang, D. Rabinovich, Inorg. Chem. 45 (2006) 5103.
[47] C.Z. Wang, Y.F. E, L.Z. Fan, Z.H. Wang, H.B. Liu, Y.L. Li, S.H. Yang, Adv. Mater 19 (2007) 3677.
[48] H. Pan, Y.P. Feng, Q.Y. Wu, Z.G. Huang, J.Y. Lin, Phys. Rev. B 77 (2008) 125211.